

Photoluminescence in transition metal dichalcogenides: Towards high quantum yield

Xin Yan(闫欣), Weijia Tang(汤唯佳), Guilong Gao(高贵龙), Kai He(何凯), Dong Yao(姚东), Butian Zhang(张卜天), Shun Wang(王顺), and Youwei Zhang(张有为)

Citation: Chin. Phys. B, 2026, 35 (**8**): 087801. DOI: 10.1088/1674-1056/ae60f1
http://cpb.iphy.ac.cn; http://iopscience.iop.org/cpb

What follows is a list of articles you may be interested in

Magnetic-field-induced photoluminescence enhancement in type-I quantum wells: A quantitative probe for interface flatness

Jun Shao(邵军), Man Wang(王嫚), Xiren Chen(陈熙仁), Liangqing Zhu(朱亮清), F. X. Zha(查访星), H. Zhao, Shumin Wang(王庶民), and Wei Lu(陆卫)

Chin. Phys. B, 2025, 34 (**10**): 107802. DOI: 10.1088/1674-1056/adf5a7

Layer-dependent exciton dynamics in InSe/WS_2 heterostructures

Siyao Li(李思垚), Yufan Wang(王雨凡), Zhiqiang Ming(明志强), Yong Liu(刘勇), Lanyu Huang(黄岚雨), Siman Liu(刘思嫚), Jialong Li(李佳龙), Yulin Chen(成昱霖), Zhoujuan Xu(徐周娟), Zeyu Liu(刘泽宇), Danliang Zhang(张丹亮), and Xiao Wang(王笑)

Chin. Phys. B, 2025, 34 (**9**): 097802. DOI: 10.1088/1674-1056/adc6f7

Effects of helium ion irradiation and thermal annealing on the optical and structural properties of hexagonal boron nitride

Guan-Lin Liu(刘冠麟), Ji-Lian Xu(徐辑廉), Peng-Tao Jing(景鹏涛), Jing-Jing Shao(邵京京), Xu Guo(郭旭), Yun-Tao Wu(吴韵涛), Feng Qin(覃凤), Zhen Cheng(程祯), Deming Liu(刘德明), Yang Bao(鲍洋), Hai Xu(徐海), Li-Gong Zhang(张立功), Da Zhan(詹达), Jia-Xu Yan(闫家旭), Lei Liu(刘雷), and De-Zhen Shen(申德振)

Chin. Phys. B, 2025, 34 (**5**): 057801. DOI: 10.1088/1674-1056/adbee7

Polarized photoluminescence spectroscopy in WS_2, WSe_2 atomic layers and heterostructures by cylindrical vector beams

Lijun Wu(吴莉君), Cuihuan Ge(葛翠环), Kai Braun, Mai He(贺迈), Siman Liu(刘思嫚), Qingjun Tong(童庆军), Xiao Wang(王笑), and Anlian Pan(潘安练)

Chin. Phys. B, 2021, 30 (**8**): 087802. DOI: 10.1088/1674-1056/abf3b6

Efficient doping modulation of monolayer WS_2 for optoelectronic applications

Xinli Ma(马新莉), Rongjie Zhang(张荣杰), Chunhua An(安春华), Sen Wu(吴森), Xiaodong Hu(胡晓东), Jing Liu(刘晶)

Chin. Phys. B, 2019, 28 (**3**): 037803. DOI: 10.1088/1674-1056/28/3/037803

REVIEW

Photoluminescence in transition metal dichalcogenides: Towards high quantum yield

Xin Yan(闫欣)[1,2,†], Weijia Tang(汤唯佳)[3,†], Guilong Gao(高贵龙)[2,‡], Kai He(何凯)[2,§], Dong Yao(姚东)[2], Butian Zhang(张卜天)[3], Shun Wang(王顺)[3], and Youwei Zhang(张有为)[3,¶]

[1] *Rocket Force University of Engineering, Xi'an* 710025, *China*

[2] *State Key Laboratory of Ultrafast Optical Science and Technology, Xi'an Institute of Optics and Precision Mechanics, Chinese Academy of Sciences, Xi'an* 710119, *China*

[3] *National Gravitation Laboratory, MOE Key Laboratory of Fundamental Physical Quantities Measurement, and School of Physics, Huazhong University of Science and Technology, Wuhan* 430074, *China*

(Received 15 March 2026; revised manuscript received 9 April 2026; accepted manuscript online 17 April 2026)

Owing to their atomic-level thickness, strong light–matter interaction, and wide range of bandgap tunability, transition metal dichalcogenides (TMDCs) hold great promise as light-emitting materials. Research on photoluminescence (PL) plays an indispensable role in the development of related fields, with efficiency being one of the most critical metrics for evaluating luminescence performance. Distinct from conventional direct-bandgap semiconductors, the unique exciton luminescence characteristics of TMDCs have established a new paradigm for investigating PL properties while simultaneously posing fresh challenges for modulating PL efficiency. Consequently, the study of PL efficiency modulation in TMDCs carries both fundamental physical significance and engineering application value. Based on an understanding of exciton physics in TMDCs, this review first summarizes strategies for enhancing PL quantum yield (QY) under low generation rates, including doping, defect engineering, interface engineering, and optical engineering. Subsequently, several strategies for suppressing exciton–exciton annihilation (EEA) under high generation rates are introduced. Finally, the current challenges are summarized, and an outlook on future development directions is provided.

Keywords: transition metal dichalcogenides (TMDCs), photoluminescence (PL), quantum yield (QY), exciton dynamics, exciton–exciton annihilation

PACS: 78.67.–n, 71.35.–y, 78.55.–m

DOI: 10.1088/1674-1056/ae60f1 **CSTR:** 32038.14.CPB.ae60f1

1. Introduction

Photoluminescent materials play an indispensable role in modern society. As one of the most important forms of luminescence, photoluminescence (PL) is not only a non-contact characterization tool of great scientific significance for studying the band structure, defect states, carrier dynamics, and excitonic behavior of materials, but also finds ubiquitous applications ranging from daily lighting and display technologies to bioimaging, medical diagnostics, and anti-counterfeiting markers. Among the plethora of emerging luminescent materials, two-dimensional transition metal dichalcogenides (TMDCs) have garnered significant attention due to their unique properties. When TMDCs such as MoS_2 and WS_2 are thinned down to a monolayer, their band structure transitions from an indirect to a direct bandgap, exhibiting a significant photoluminescence enhancement.[1] TMDCs possess good thermal and chemical stability, with a tunable bandgap in the range of 1–2 eV covering the visible to near-infrared spectral region.[2,3] Their optical absorption coefficient is an order of magnitude higher than that of conventional semiconductors,[4] laying a solid foundation for achieving efficient photoluminescence.

The pursuit of efficiency is an eternal theme in the development of luminescent materials. For traditional II–VI and III–V direct bandgap semiconductors (e.g., GaAs, InGaN), the photoluminescence quantum yield (PL QY) is given by PL QY $= \gamma_r/(\gamma_r+\gamma_{nr})$, where γ_r is the radiative recombination rate and γ_{nr} is the non-radiative recombination rate. Therefore, the key to increasing the luminescence efficiency lies in improving crystal quality to reduce the density of defects that act as non-radiative recombination centers.[5] Different from the interband recombination of free carriers in bulk direct bandgap semiconductors, the luminescence of monolayer TMDCs is predominantly governed by excitons due to the strong quantum confinement and weak dielectric screening arising from their atomic thickness.[6] The exciton bind-

[†]These authors contributed equally to this work.
[‡]Corresponding author. E-mail: gaoguilong@opt.ac.cn
[§]Corresponding author. E-mail: hekai@opt.ac.cn
[¶]Corresponding author. E-mail: youweizhang@hust.edu.cn

© 2026 Chinese Physical Society and IOP Publishing Ltd. All rights, including for text and data mining, AI training, and similar technologies, are reserved.

ing energies in TMDCs are as high as several hundred millielectronvolts, more than an order of magnitude larger than those in traditional quantum well structures.[7–9] This allows excitons and their complexes to exist stably at room temperature and dominate the luminescence mechanism. Consequently, for TMDCs, the PL QY can be expressed as PL QY $= \alpha \times \gamma_r/(\gamma_r + \gamma_{nr})$, where α is the exciton formation probability, whose physical meaning lies in distinguishing the two independent processes of "exciton formation" and "exciton recombination". α measures the proportion of carriers that are effectively converted into exciton states before undergoing ultrafast trapping (by defects) or direct non-radiative recombination. Experimentally, α is difficult to measure directly but can be indirectly extracted by capturing the dynamics of carrier conversion into exciton states using time-resolved photoluminescence spectroscopy, combined with rate equation modeling.[10] Precisely because of this exciton-dominated luminescence characteristic, defects are no longer the sole dominant factor affecting the PL QY.[11] On one hand, this relaxes the stringent requirements for material preparation; on the other hand, it results in significant differences in the strategies for modulating the PL QY of TMDCs compared to conventional semiconductor materials. This distinction makes the study of luminescence efficiency modulation not only conducive to revealing exciton dynamics, defect-interface interactions, and many-body physical mechanisms, thereby enriching fundamental research in low-dimensional material systems, but also of great engineering value, helping to unlock the potential of TMDCs in the fields of valleytronics, quantum information, and low-power optoelectronics.

TMDCs host a rich variety of excitonic species, including neutral excitons, trions, biexcitons, and bound excitons,[12–15] each with different binding energies and therefore different formation probabilities. Furthermore, the exciton formation probability is governed by multiple factors, including: the transition of exciton types induced by doping, many-body screening under high carrier density, scattering introduced by exciton–phonon interactions, carrier trapping by defects and local potentials, the introduction of bright/dark excitons due to spin and valley selection rules, strain-induced changes in band structure and carrier effective mass, the local electric field strength in plasmonic structures and whether the excitation energy satisfies resonant conditions. Naturally, the γ_r and γ_{nr} also vary depending on the exciton species. The Purcell effect, achieved by modifying the optical environment, and strain engineering are considered effective means to modulate the γ_r. In contrast, the γ_{nr} is more sensitive to defects and exciton density. Particularly under high exciton concentration, exciton–exciton annihilation (EEA) becomes the dominant non-radiative recombination mechanism. Additionally, the α, γ_r, and γ_{nr} are collectively influenced by external environmental factors, including: dielectric screening and interfacial phonon scattering induced by the substrate and encapsulation environment, as well as thermal perturbation and changes in bright/dark exciton distribution caused by temperature. These factors ultimately modulate the PL QY by influencing α, γ_r, and γ_{nr}, as illustrated in Fig. 1.

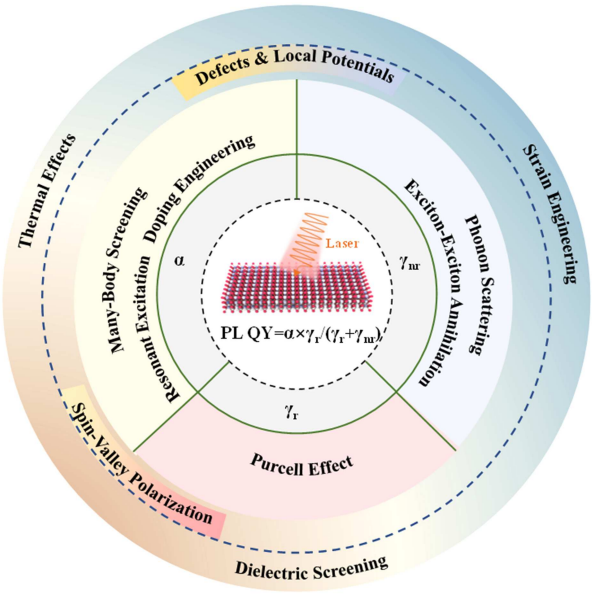


Fig. 1. Schematic illustration of the various factors that influence the α, γ_r, and γ_{nr}, thereby determining the PL QY in TMDCs.

Given the diverse excitonic species and complex recombination mechanisms in monolayer TMDCs, this review will first elucidate the excitonic physics in monolayer TMDCs and its impact on luminescence properties (Section 2). Subsequently, according to the two regimes of low and high generation rates, various strategies for enhancing the PL QY will be systematically discussed: under low generation rates, the focus will be on chemical doping, electrostatic doping, defect engineering, interface engineering and optical engineering (Section 3); under high generation rates, the focus will shift to methods for suppressing exciton–exciton annihilation, including hBN encapsulation, metallic screening, and strain engineering (Section 4). Finally, a summary and outlook will be provided (Section 5).

2. Excitonic complexes in TMDCs

The weak dielectric screening and strong geometric confinement in TMDCs result in extremely strong Coulomb interactions between charge carriers, leading to the formation of various quasi-particles known as excitons,[6,11,16–18] as illustrated in Fig. 2(a). Firstly, neutral excitons are formed by the Coulomb interaction between an electron–hole pair. This is followed by charged excitons (trions), which carry positive or negative charges and are formed by the binding of a neutral exciton with an additional electron or hole. Furthermore, when excitons are trapped by lattice defects, they give rise to bound excitons. Additionally, higher-order excitonic

derivatives exist, such as biexcitons, which emerge from interactions between excitons.[12,13] Finally, in van der Waals heterostructures composed of different TMDCs, electrons and holes originating from different TMDC layers can form a new type of exciton under Coulomb interaction, known as interlayer excitons.[14,15]

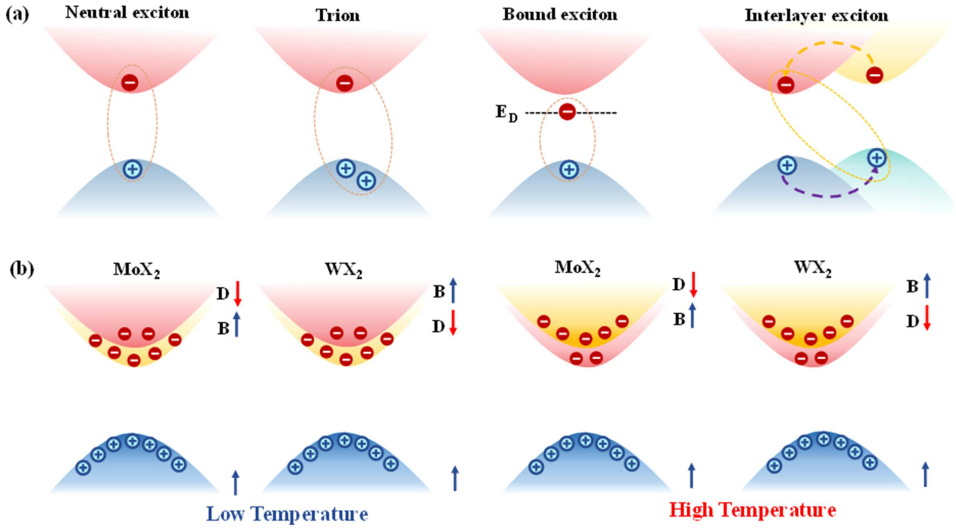


Fig. 2. (a) Illustration of different exciton types in TMDCs, with ED indicating defect energy levels. (b) Schematic diagram of thermal redistribution of spin-allowed bright excitons (B) and spin-forbidden dark excitons (D) of MoX_2 and WX_2 at low temperature and high temperature. Red arrows indicate spin-down, blue arrows indicate spin-up. Adapted with permission from Refs. [6,11–18].

2.1. Neutral excitons

Neutral excitons refer to bound states composed of an electron and a hole, where their respective charges cancel each other, rendering the entity electrically neutral. When the concentrations of positive and negative carriers are balanced, neutral excitons dominate the excitonic population. In monolayer TMDCs, due to the lack of inversion symmetry and strong spin–orbit coupling, the valence band maximum exhibits an energy splitting of approximately 150–500 meV.[19] This splitting gives rise to lower-energy A excitons and higher-energy B excitons. Since luminescence in TMDCs is dominated by A excitons, the excitons discussed in this review refer specifically to A excitons. Similarly, spin–orbit coupling induces a spin splitting of several tens of meV at the bottom of the conduction band in TMDCs.[19–21] Electrons in these two spin-split conduction band levels possess opposite spin directions and can each bind with a hole in the valence band via Coulomb interactions to form neutral excitons. These excitons are classified as spin-allowed bright excitons and spin-forbidden dark excitons. The differences between bright and dark excitons obviously have a significant impact on the luminescence performance of TMDCs. As illustrated in Fig. 2(b), in MoX_2 (X = S, Se, Te), the lowest energy state is a bright exciton due to the aligned spins of carriers at the conduction band minimum and valence band maximum. Conversely, in WX_2 (X = S, Se), the lowest energy state is a dark exciton. Considering the thermal redistribution of exciton populations, the radiative recombination rates of excitons in MoX_2 and WX_2 exhibit opposing temperature dependencies.[21] This behavior offers opportunities for designing TMDC-based light-emitting devices tailored to specific temperature environments. On the other hand, to enhance the radiative recombination rates of dark excitons in WX_2, researchers have proposed strategies such as applying external magnetic fields and employing plasmonic methods.[22]

2.2. Trions

In TMDCs, the weak charge screening and large carrier effective mass significantly enhance the Coulomb interaction between charges. When excess carriers are present, neutral excitons tend to bind with background carriers under Coulomb forces, forming charged excitons known as trions, which lowers the system's overall energy.[23] The probability of trion formation is positively correlated with the doping concentration in TMDCs. Meanwhile, TMDCs are usually in a doped state due to intrinsic material defects, such as vacancies and impurities, as well as external environmental influences, including adsorbates and dielectric interfaces.[24] The binding energy of trions in monolayer TMDCs is approximately 30 meV, comparable to the thermal ionization energy at room temperature ($\sim$ 26 meV) and an order of magnitude larger than that in traditional quasi-2D semiconductor systems, such as quantum wells.[23] The presence of trions markedly affects the luminescence properties of TMDC materials. Experimental studies on monolayer MoS_2 revealed that the PL intensity ratio of trions to neutral excitons is strongly dependent on temperature and doping concentration.[12,25,26] At room temperature, negative trions dominate the A exciton emission peak in exfoliated monolayer MoS_2, with their proportion increasing as temperature decreases, indicating that trions play an important role in the luminescence characteristics of TMDCs.

2.3. Interlayer excitons

With the emergence of vertically stacked heterostructures, excitonic physics in TMDCs has become increasingly complex and diverse. Excitons can be categorized based on the spatial positions of the electron and hole as intralayer excitons or interlayer excitons. Intralayer excitons refer to electron–hole pairs that are bound within the same TMDC layer. In TMDCs heterostructures, band alignment offsets drive electrons and holes to separate into different TMDC layers, where they are bound by Coulomb forces to form interlayer excitons.[14,26–32] The binding energy of interlayer excitons in TMDCs heterostructures ranges around 100 meV,[33,34] enabling their stable existence at room temperature. Compared to intralayer excitons in monolayer TMDCs, the spatial separation of electrons and holes significantly reduces wavefunction overlap, resulting in a much longer exciton lifetime.[14,35] However, due to unavoidable lattice mismatch and/or interlayer twist, electrons and holes in interlayer excitons often experience momentum mismatch, making the interlayer exciton optically dark.[36] Consequently, radiative recombination of interlayer excitons requires phonon assistance, significantly lowering their recombination efficiency. Additionally, the spatial separation of charge carriers leads to quenching of intralayer exciton emission.[37] These characteristics collectively render TMDCs heterostructures less suitable for developing high-brightness light-emitting devices.

2.4. Bound excitons

The presence of impurities or defects in semiconductors generates defect states, which act as localized potential traps that capture excitons, leading to the formation of bound excitons, also known as localized excitons.[11,38–41] In intrinsic TMDCs, the low defect density and the large laser spot size used in far-field PL spectroscopy typically prevent the observation of bound exciton luminescence at room temperature.[42,43] However, as the temperature decreases, the emission peaks of these localized excitons become increasingly prominent. Under low temperature and low excitation power conditions, bound exciton emission can even become the dominant luminescence mechanism in TMDCs. This phenomenon has been observed in monolayer MoS_2,[44] WS_2,[45] WSe_2[42] and $MoSe_2$.[46] On the other hand, artificial defect engineering using techniques such as electron beam irradiation,[47] plasma treatment[48] and UV exposure[49] can intentionally introduce defects in TMDCs, increasing defect density and potentially enabling the observation of bound exciton luminescence peaks even at room temperature.[49]

3. QY enhancing strategies under low generation rate

Among the aforementioned exciton species, interlayer excitons are optically dark. Additionally, bound exciton emission only becomes dominant at extremely low temperatures or under high defect densities, making it less ideal for realizing high-brightness PL. Therefore, in TMDCs, the QY is collectively determined by the proportions of neutral excitons and trions, as well as their respective α, γ_r, and γ_{nr}. This section will systematically review various enhancement strategies developed in recent years according to this framework, clarifying the dominant influence of each strategy on the three parameters mentioned above. Unlike in bulk semiconductors, where Auger recombination predominantly limits QY at high carrier injection levels,[50] in TMDCs, the main factor leading to QY degradation under high generation rates is EEA.[51–53] Consequently, based on the exciton generation rate, we will first introduce QY-enhancing strategies under low generation rates in this section, and subsequently discuss in the next section the strategies for suppressing EEA under high generation rates. Table 1 summarizes the PL properties of TMDCs under various modulation methods reported in previous studies.

Under low generation rates, the exciton density is low, leading to weak exciton–exciton interactions. Consequently, carrier recombination is primarily dominated by single neutral excitons or trions. The non-radiative recombination process of trions is three orders of magnitude faster than the radiative recombination process; thus, non-radiative recombination dominates in the trion recombination mechanism.[11] The formation of trions is related to the carrier concentration in TMDCs, which is influenced by material defects such as vacancies and impurities, as well as external factors including electrostatic fields, dielectric interfaces, and surface modification layers. On the other hand, sulfur-based TMDCs and selenide-based TMDCs exhibit significant differences in defect types: sulfur-based TMDCs predominantly feature simple sulfur vacancies, whereas selenide-based TMDCs possess more complex defects.[54,55] This disparity results in distinct radiative recombination efficiencies for neutral excitons in these two categories of TMDCs.[11,54] Specifically, the radiative recombination efficiency of neutral excitons in sulfur-based TMDCs is significantly higher than that in selenide-based TMDCs. For inherently N-type doped sulfur-based TMDCs, researchers have proposed various techniques to enhance the QY of TMDCs through strategies such as chemical doping, electrostatic doping, defect engineering, and interface engineering. As a result, nearly 100% PL QY has been successfully achieved under low generation rates.[11,54,56] In contrast, for nearly intrinsic selenide-based TMDCs with very low carrier concentrations, doping treatments have proven ineffective in enhancing PL QY. Instead, defect engineering and interface engineering emerge as promising approaches for improving PL QY.[57,58]

Table 1. A summary of PL enhancement strategies in TMDCs. RT stands for room temperature.

Low generation rate						
Enhancement strategies	Active material	PL QY	Wavelength	Temperature	Maximum PL enhancement	Ref.
Chemical treatment doping	MoS_2	Near 100%	660 nm	RT	950-fold	[56]
Chemical treatment doping	MoS_2	\	660 nm	RT	2-fold	[64]
Chemical treatment doping	$MoSe_2$		795 nm	RT	30-fold	[65]
Chemical treatment doping	MoS_2		660 nm	RT	3-fold	[66]
Chemical treatment doping	MoS_2		660 nm	RT	35-fold	[67]
Chemical treatment doping	$MoSe_2$		795 nm	RT	30-fold	[67]
Electrostatic doping	MoS_2	Near 100%	660 nm	RT	750-fold	[11]
Electrostatic doping	WS_2	90%	620 nm	RT		[11]
Electrostatic doping	MoS_2		660 nm	RT	100-fold	[72]
Electrostatic doping	MoS_2		660 nm	RT	3-fold	[85]
Defect engineering	MoS_2		660 nm	RT	200-fold	[88]
Defect engineering	MoS_2		670 nm	RT	100-fold	[89]
Defect engineering	WS_2	9.3%	620 nm	RT	10-fold	[90]
Defect engineering	$MoSe_2$		794 nm	RT	58-fold	[58]
Defect engineering	$MoSe_2$		810 nm	RT	30-fold	[65]
Defect engineering	WS_2		618 nm	RT	27-fold	[83]
Defect engineering	MoS_2		678 nm	RT	89-fold	[91]
Defect engineering	MoS_2		660 nm	RT	275-fold	[93]
Defect engineering	MoS_2		670 nm	RT		[94]
Interface engineering	MoS_2	4.1%	660 nm	RT	30-fold	[98]
Interface engineering	WS_2	40%	620 nm	RT	17-fold	[98]
Interface engineering	WSe_2	22%	750 nm	RT	37-fold	[98]
Interface engineering	MoS_2		652 nm	RT	20-fold	[102]
Interface engineering	MoS_2		670 nm	RT	4-fold	[102]
Interface engineering	WSe_2	60%	751 nm	RT	20-fold	[57]
Optical engineering	WSe_2		710 nm	77 K	7-fold	[105]
Optical engineering	MoS_2		660 nm	RT	22-fold	[106]
Optical engineering	MoS_2		675 nm	RT	4.5-fold	[107]
Optical engineering	$MoSe_2$		789 nm	RT	1840-fold	[111]
Optical engineering	WSe_2		750 nm	RT	18000-fold	[108]
Optical engineering	WS_2		633 nm	RT	1265-fold	[110]
High generation rate						
Enhancement strategies	Active material	QY	Wavelength	Temperature	Maximum PL enhancement	Ref.
hBN encapsulation	WS_2		623 nm	RT	10-fold	[116]
Metallic screening	WS_2		623 nm	RT	18-fold	[51]
Uniform strain engineering	WSe_2	Near 100%	770 nm	RT	100-fold	[117]
Uniform strain engineering	WS_2	Near 100%	623 nm	RT		[117]
Strain gradient engineering	WS_2	50%	620 nm	RT		[118]
Strain gradient engineering	WSe_2	47%	710 nm	4 K		[119]

3.1. Chemical treatment doping

When external molecules are introduced onto the surface of TMDCs as dopants, charge transfer spontaneously occurs between the TMDCs and the dopants due to differences in their energy levels. When the Fermi level/work function/electrochemical potential/electron affinity of the dopant molecules is lower than that of the TMDCs, electrons transfer from the TMDCs to the dopants, leading to P-type doping of the TMDCs.[59,60] Conversely, when this energy parameter is higher, electrons transfer from the dopants to the TMDCs, resulting in N-type doping. 2D TMDCs possess a large specific surface area and nanometer-scale thickness, making them particularly suitable for modulating carrier concentration and polarity via this method. In TMDCs, when the carrier polarity and concentration change, the respective α of neutral excitons and trions vary accordingly, thereby affecting the relative proportion of the two exciton species. Combined with the fact that neutral excitons and trions themselves have different γ_r and γ_{nr}, these changes collectively determine the PL QY. Numerous studies have reported the enhancement of PL through chemical doping.[38,54,61–63]

In 2015, Amani *et al.* reported a method involving the treatment of ML MoS_2 with a non-oxidizing organic superacid, bis(trifluoromethanesulfonyl)imide (TFSI), which resulted in significant PL enhancement.[56] Figure 3(a) presents the PL spectra before and after TFSI treatment, clearly demonstrating a substantial increase in PL intensity following the

treatment. Under identical conditions, TFSI treatment elevated the PL QY by two orders of magnitude at low generation rate, as shown in Fig. 3(b), approaching a value of 1. The authors initially posited that TFSI might passivate electronically active defect sites in ML MoS_2, thereby mitigating defect-induced non-radiative recombination. However, subsequent studies by the same research group demonstrated that TFSI functions as a Lewis acid rather than a defect passivator.[11] By withdrawing electrons from TMDCs via surface charge transfer, TFSI reduces the excess electron concentration in TMDCs, increases the proportion of neutral excitons, and ultimately enhances the PL QY. Nevertheless, the harsh nature of the TFSI superacid restricts its practical application in optoelectronic devices.

In 2021, Li *et al*. discovered that a chemically milder TFSI anion-based ionic salt could also achieve P-type doping, suppressing trion emission and enhancing PL.[61] The authors treated monolayer WS_2 with various chemical agents and compared their PL enhancement effects, as shown in Fig. 3(c), where Li-TFSI exhibited the most pronounced PL enhancement. Following this rationale, doping TMDCs with two opposite-polarity dopants should result in opposite effects on their PL intensity. A study by Zhang *et al*. in 2018 confirmed this hypothesis.[64] They found that the PL intensity of MoS_2 could be enhanced through P-type doping using "Magic Blue", $[N(C_6H_4\text{-p-Br})_3]SbCl_6$, whereas N-type doping with pentamethylrhodocene dimer quenched the PL emission. Furthermore, research has identified hydrohalic acids,[65] 2,3,5,6-tetrafluoro 7,7,8,8-tetracyanoquinodimethane (F_4TCNQ),[38,66] H_2O_2,[63] O_2 and/or H_2O[67] as electron-withdrawing dopants, each contributing to an increase in PL QY to varying extents.

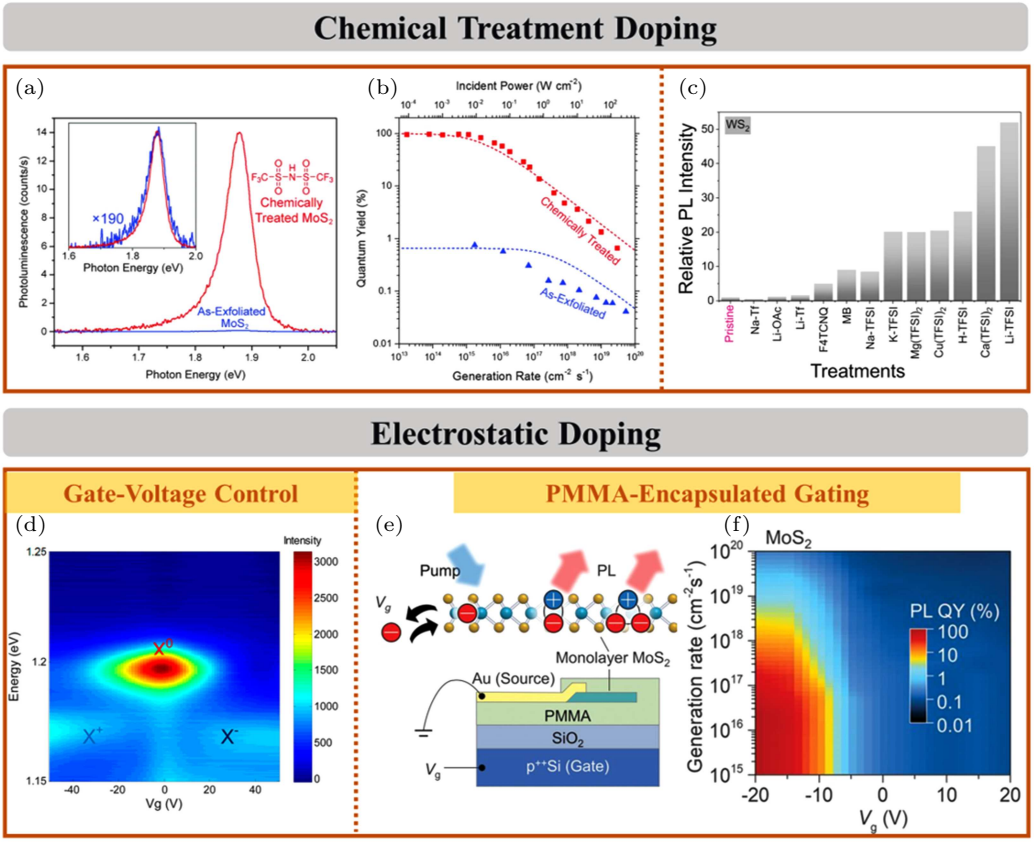


Fig. 3. (a) PL spectra of as-exfoliated and TFSI-treated monolayer MoS_2 at an incident power of 1×10^{-2} W·cm^{-2}, with the inset showing the normalized spectra. (b) Generation rate dependence of PL QY for as-exfoliated and TFSI chemically treated MoS_2. (c) Comparison of PL intensity enhancement in WS_2 under different chemical treatments, with the pristine sample's PL intensity normalized to 1. (d) Color plot of the PL spectra of 1L $MoTe_2$ as a function of gate voltage (V_g). In the figure, X^0, X^+, and X^- represent the emission from neutral excitons, positively charged excitons, and negatively charged excitons, respectively. (e) Schematic illustration of the MOS capacitor device structure. (f) Color plot of PL QY of 1L MoS_2 as a function of V_g and generation rate. Reproduced with permission from Refs. [11,56,61,74].

3.2. Electrostatic doping

Compared with conventional 3D semiconductor materials, the inherent 2D nature of TMDCs and their relatively weak charge screening effects make their carrier type and concentration highly susceptible to external electric field modulation.[68–70] Similar to chemical doping, this strategy also changes the relative proportion of neutral excitons and trions by affecting their respective α, thereby influencing γ_r and γ_{nr}, which ultimately determines PL QY. Around 2012, researchers employed field-effect transistors (FETs) to investigate the influence of gate voltage on the PL emission of TMDCs.[11,71–73] They observed that the PL intensity of monolayer MoS_2 exhibits a pronounced dependence on the electric field, with the intensity increasing by up to three or-

ders of magnitude as the gate voltage shifts from negative to positive. Beyond MoS_2, other TMDCs such as WSe_2, WS_2, and $MoTe_2$ also exhibited gate voltage-dependent PL emission.[74–76] The reason for the gate voltage dependence of the PL intensity is usually attributed to the modulation of neutral exciton emission weight by electrostatic doping,[11,68,75,76] as depicted in Fig. 3(d). When a high carrier concentration is introduced via electrostatic doping, neutral exciton emission is suppressed, favoring charged exciton emission and resulting in reduced PL intensity. Conversely, when the carrier concentration in TMDCs is low, the proportion of neutral excitons increases, enhancing PL emission. This suggests that some researchers had already recognized the higher radiative recombination efficiency of neutral excitons compared to charged excitons, although no studies had systematically compared the radiative recombination efficiencies of the two exciton types at that time.

In 2019, Lien *et al*. quantitatively explored the effect of gate voltage on the PL QY of TMDCs by constructing a metal–oxide–semiconductor (MOS) capacitor.[11] To mitigate the influence of ionized impurities at the gate dielectric interface and adsorbed species from the environment, unlike previous studies that typically utilized back-gated FET structures, the researchers encapsulated TMDCs within poly(methyl methacrylate) (PMMA) and transferred gold electrodes to establish electrical connections, thereby forming an MOS capacitor (Fig. 3(e)). Using this structure, they quantitatively assessed the impact of gate voltage on the PL QY of TMDCs. Figure 3(f) presents the PL QY of MoS_2 under different gate voltages and generation rates, revealing that even without any chemical passivation, monolayer MoS_2 and WS_2 can achieve near-unity PL QY. Although prior chemical treatment doping had already enabled near-unity PL QY in monolayer MoS_2 and WS_2,[54,56] such treatments might involve not only doping effects but also the repair or passivation of defects in TMDCs by molecules or ions, which could also affect exciton radiative recombination efficiency. Given that the exfoliated TMDCs exhibit defect densities ranging from 10^{10} cm^{-2} to 10^{13} cm^{-2}, Lien *et al*.'s work provided the first unambiguous evidence that defects in monolayer MoS_2 and WS_2 have no detrimental effect on the radiative recombination of neutral excitons, indicating that neutral exciton recombination is entirely radiative.[77] This marks a significant departure from traditional inorganic semiconductors, where even a small number of defects can act as nonradiative recombination centers and adversely affect the luminescence properties of the material.[5] Under low injection conditions, non-radiative recombination is predominantly governed by defect-related Shockley–Read–Hall (SRH) recombination.[50] Consequently, efforts to enhance luminescence efficiency in II–VI and III-V direct bandgap semiconductors have primarily focused on reducing defect densities, particularly dislocations.[78–81]

However, it should be noted that in Lien *et al*.'s study, the defects in monolayer MoS_2 and WS_2 are predominantly sulfur vacancies, thus only demonstrating that the radiative recombination efficiency of neutral excitons is insensitive to sulfur vacancies. On the other hand, defects in TMDCs encompass multiple types, closely linked to the material type and fabrication process.[82] Possibly due to the fact that defects in selenide-based TMDCs are not simply chalcogen vacancies, neither TFSI treatment nor electrostatic doping can enhance the PL QY of selenide-based TMDCs.[54] Even in sulfur-based TMDCs, differences in material synthesis methods may lead to variations in defect types, and other research groups have found that using TFSI for P-type doping alone has a limited effect on improving PL QY.[61,83] Therefore, defect engineering is necessary to repair or passivate defects that reduce the radiative recombination efficiency of neutral excitons. The subsequent section will address content related to defect engineering. Although electrostatic doping avoids the instability issues associated with chemical treatments and is beneficial for applications in optoelectronic devices, conventional electrostatic doping is volatile, requiring a continuous voltage input to maintain the doped state of TMDCs. In contrast, ferroelectric polarization offers advantages such as non-volatility, low power consumption, and high integration density.[84] In 2024, Pucher *et al*. integrated monolayer MoS_2 with $BaTiO_3$ (BTO), leveraging the electrostatic field induced by BTO's ferroelectric polarization to alter the doping level of MoS_2, thereby achieving modulation of PL emission intensity.[85]

3.3. Defect engineering

Defects in semiconductors generally refer to disruptions or interruptions in the periodic arrangement of the crystal lattice, resulting in structural anomalies or imperfections. Common types of defects in TMDCs include vacancies, impurities, interstitial defects, and antisite defects.[77,86] The nature of these defects is closely related to the elemental composition of TMDCs as well as the fabrication methods used for crystal growth.[82,87] Accordingly, defect engineering approaches to enhancing the PL QY of TMDCs can be classified into two distinct technical approaches. The first technical approach involves elemental substitution doping to improve PL QY.[88–90] Similar to chemical and electrostatic doping, substitutional doping effectively modulates the background carrier concentration in TMDCs, thereby reducing the α of trions and utilizing the higher γ_r of neutral excitons to enhance PL QY. For example, Chen *et al*. achieved strontium (Sr) doping in MoS_2 via chemical vapor deposition (CVD),[89] as shown in Figs. 4(a) and 4(b). In this process, Sr atoms replaced Mo atoms, introducing defect levels that acted synergistically with the intrinsic defect states of MoS_2 to neutralize excess elec-

trons, thereby suppressing trion formation and significantly enhancing the PL intensity (Fig. 4(c)). Additionally, Wei *et al*. demonstrated that annealing monolayer MoS_2 samples in air at temperatures ranging from 200 °C to 400 °C led to a significant enhancement in PL intensity.[88] This enhancement arises from the substitution of sulfur (S) atoms with oxygen (O) atoms during annealing, resulting in p-type doping.

The second technical approach focuses on repairing or passivating defects to enhance PL emission.[58,65,83,91–93] The mechanisms underlying PL enhancement vary depending on the type of defect and the chemical modification molecule employed. For sulfur-based TMDCs, annealing in a sulfur vapor environment can directly fill sulfur vacancies, reducing the excess electrons introduced by these vacancies and thereby increasing PL intensity.[94] In this case, the PL enhancement mechanism is the same as that of elemental substitution doping. On the other hand, Tanoh *et al*. discovered that oleic acid (OA) treatment significantly improves the PL QY of $MoSe_2$.[58] The researchers believe that the enhancement of PL stems from OA passivating chalcogen vacancy defects by coordinating with molybdenum (Mo) dangling bonds, thereby suppressing non-radiative recombination at defect states, rather than originating from chemical doping induced by OA (Fig. 4(d)). Additionally, OA forms an insulating protective layer on the $MoSe_2$ surface, functioning similarly to hexagonal boron nitride (hBN) encapsulation. This layer minimizes doping effects from atmospheric O_2 and H_2O, thereby reducing trap states induced by adsorbed external molecules. A comparison of $MoSe_2$ PL before and after OA treatment (Fig. 4(e)) shows that the PL intensity of $MoSe_2$ increased by approximately 60-fold after OA treatment. Furthermore, researchers have found that poly(4-styrenesulfonate) (PSS) can also significantly enhance the PL of TMDCs by repairing sulfur vacancies; however, PSS treatment also alters the doping state of TMDCs, suggesting that the observed PL enhancement may also include contributions from chemical doping.[92] Therefore, combining defect passivation with doping could be a highly promising strategy for improving PL QY. In this context, the change in PL QY arises not only from the alteration of the respective α of neutral excitons and trions, but also from the suppression of γ_{nr} for both exciton species by passivation. Bretscher *et al*. demonstrated that sequential treatment using a passivating agent (PA), such as thiols or sulfides, followed by TFSI treatment to remove excess electrons, resulted in a 275-fold enhancement in PL, an improvement superior to that achieved using TFSI chemical doping alone (Fig. 4(f)).[93]

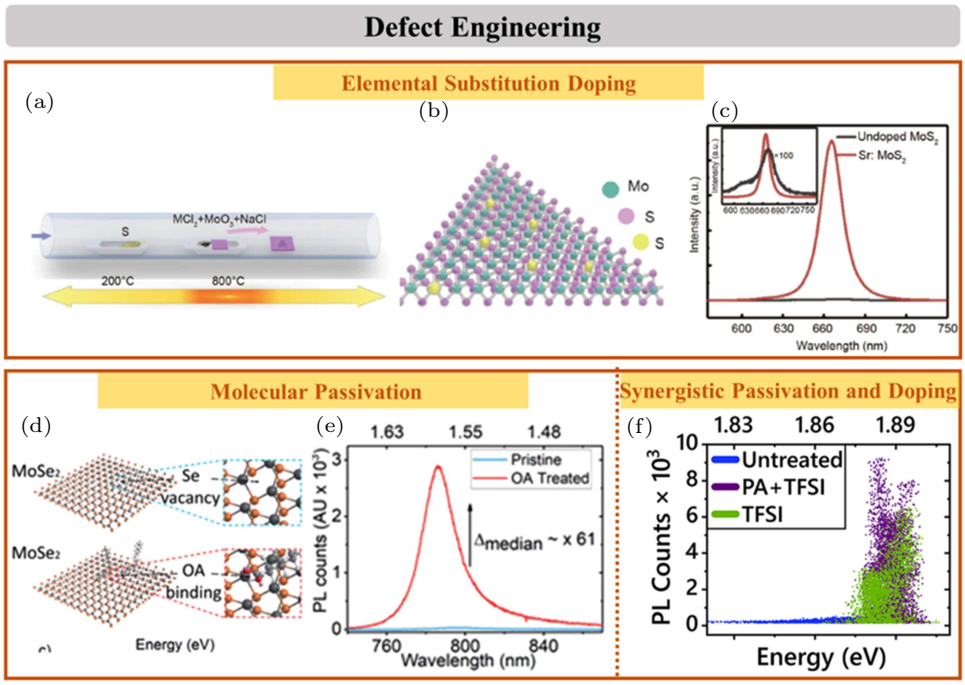


Fig. 4. (a) and (b) Schematic illustration of the preparation process and atomic structure of Sr-doped monolayer MoS_2. (c) PL spectra of undoped MoS_2 and Sr-doped MoS_2. The inset shows the intensity-normalized spectra. (d) Schematic diagram of OA ligand coordination with Se vacancies. (e) Comparison of PL emission intensity between pristine monolayer $MoSe_2$ (blue) and OA-treated monolayer $MoSe_2$ (red). (f) Comparison of PL emission intensity for untreated MoS_2 and MoS_2 treated with TFSI and PA+TFSI. Reproduced with permission from Refs. [58,89,93].

3.4. Interface engineering

Due to the atomic-scale thickness of TMDCs, their physical properties are highly sensitive to the interfacial conditions. The interfacial environment can influence the PL emission of TMDCs through multiple mechanisms. First, the dielectric environment, including both the substrate and the capping layers, can induce doping effects through surface charge transfer between the TMDCs and the surrounding media.[95–97] The

presence of ionized impurities in commonly used oxide substrates, such as SiO_2, introduces significant N-type doping in TMDCs, thereby increasing the trion population and reducing the PL intensity.[95] Therefore, increasing the spacing between the TMDCs and the oxide substrate or inserting spacer layers with weaker doping effects, such as hBN[95] or mica,[98] can markedly mitigate substrate-induced doping, thereby increasing the α of neutral excitons and ultimately enhancing the PL intensity.

In 2016, Yu *et al.* fabricated prepatterned hole structures on SiO_2/Si substrates and found that, for both selenide-based and sulfur-based TMDCs, the PL intensity in the suspended regions was significantly enhanced compared to the supported regions, with increases of up to two orders of magnitude (Figs. 5(a) and 5(b)).[98] They observed that although the suspended configuration effectively avoids substrate-induced doping, the enhancement in PL intensity cannot be solely attributed to changes in doping levels. Furthermore, Yu *et al.* employed various substrates, including mica, hBN, and sapphire, to compare their effects on the PL intensity of monolayer MoS_2, as depicted in Fig. 5(c). Compared to suspended structures, mica-supported MoS_2 exhibited similar PL emission characteristics in terms of spectral peak broadening and the ratio of neutral exciton to trion emission, suggesting comparable doping levels between suspended and mica-supported MoS_2. Nevertheless, the PL QY of the mica-supported sample was lower by an order of magnitude. This reflects the second pathway of dielectric-mediated luminescence modulation in TMDCs: interfacial phonon–electron interactions.[99] Temperature-dependent PL measurements have shown that electron–phonon interactions can significantly alter the non-radiative recombination rate,[100,101] with defects potentially playing a critical role in this process.[97,98]

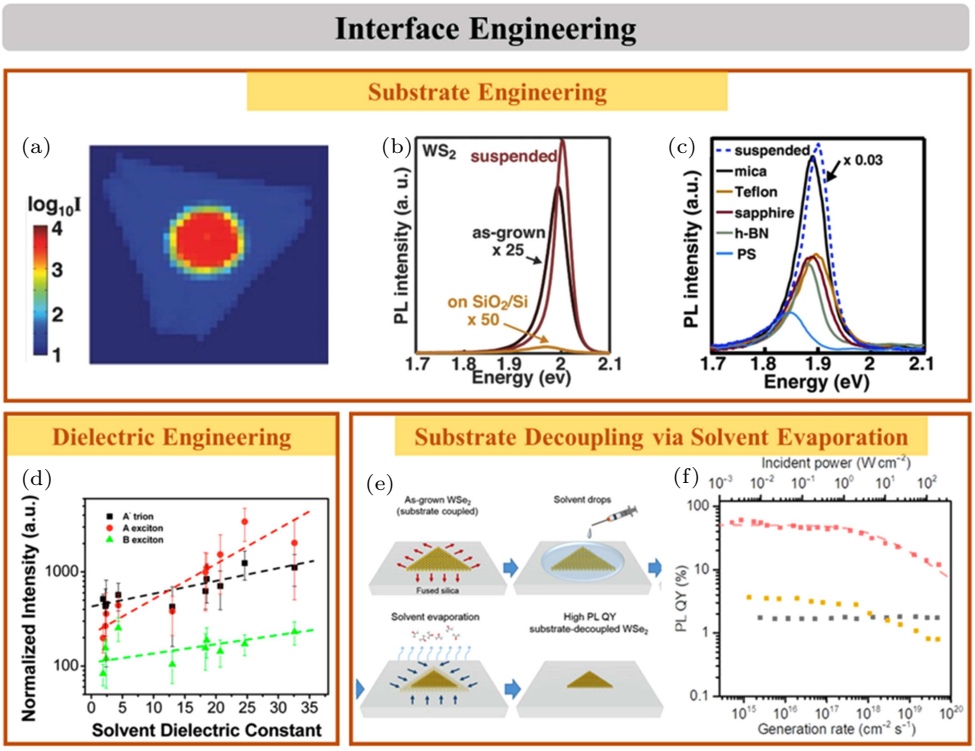


Fig. 5. (a) PL mapping of suspended monolayer TMDCs. (b) PL spectra of monolayer WS_2 under three conditions: as-grown, suspended, and transferred onto a SiO_2/Si substrate. For clarity, the PL intensities of the as-grown and transferred WS_2 are multiplied by 25 and 50, respectively. (c) PL spectra of monolayer MoS_2 grown on sapphire substrate (red) and transferred to mica (black), h-BN (gray), Teflon (orange), and polystyrene (PS) (blue) substrates. The PL spectrum of suspended monolayer MoS_2 is also shown, with its intensity multiplied by 0.03. (d) Normalized PL intensity as a function of solvent dielectric constant, where data points and error bars represent experimental measurements, and the dashed line serves as a reference. (e) Schematic of the solvent evaporation-mediated decoupling (SEMD) process. (f) PL QY as a function of generation rate for as-exfoliated, as-grown, and substrate-decoupled as-grown WSe_2. Reproduced with permission from Refs. [57,98,102].

Thirdly, the dielectric screening effect of surrounding materials can influence the Coulomb interactions between electrons and holes within excitons as well as the scattering between excitons and ionized impurities. Therefore, increasing the dielectric constant of the substrate or capping layers is expected to screen interface charge traps, reduce γ_{hr}, and thereby prolong exciton lifetimes and enhance PL emission. In a 2014 study by Lin *et al.*,[102] monolayer MoS_2 on SiO_2 substrates was immersed in solvents with varying dielectric constants, and it was found that the PL intensity increased significantly with the solvent's dielectric constant, as shown in Fig. 5(d). Finally, disparities in thermal expansion coefficients between TMDCs and substrate materials often introduce strain during the growth and fabrication processes, particularly in samples synthesized via CVD.[57,103] Strain can alter the band structure, thereby affecting the γ_r of excitons.[104] In 2019, Kim *et*

al. demonstrated that substrate decoupling via solvent evaporation could release the strain induced during the growth process,[57] as illustrated in Fig. 5(e). This method significantly enhanced the PL emission of CVD-grown WSe_2. As shown in Fig. 5(f), the PL QY of monolayer WSe_2 processed via this method exceeded that of mechanically exfoliated samples by an order of magnitude, reaching 60%. It should be noted that substrate decoupling not only releases strain but also modifies other interfacial effects such as doping and surface phonon coupling, and these factors may also contribute to the enhancement of PL QY.

3.5. Optical engineering

3.5.1. Purcell enhancement

Coupling TMDCs with optical microcavities or plasmonic nanostructures can significantly enhance their PL intensity through the Purcell effect. The essence of the Purcell effect lies in utilizing a high local photonic density of states (LP-DOS) to accelerate the radiative recombination rate, allowing it to dominate in the competition against non-radiative recombination processes. Luo *et al*. designed circular Bragg grating (CBG) cavities specifically matched to the emission frequency of WSe_2 (Figs. 6(a) and 6(b)).[105] Since Bragg reflection and cavity resonance enhancement can dramatically increase the LPDOS within the cavity, triggering a significant Purcell effect, this structure enhanced the PL intensity of WSe_2 by approximately 3-fold at room temperature and up to 7-fold at 77 K. Beyond optical microcavities, plasmonics can also increase the LPDOS. Kim *et al*. transferred few-layer MoS_2 onto pre-fabricated gold nanostructure arrays and investigated the resulting impact on MoS_2 PL (as shown in Figs. 6(c) and 6(d)).[106] The study revealed that even when the localized surface plasmon resonance (LSPR) frequency of the metallic nanostructures exhibited a significant redshift detuning relative to the excitation wavelength, the PL still showed a roughly 10-fold enhancement, primarily attributed to the Purcell effect.

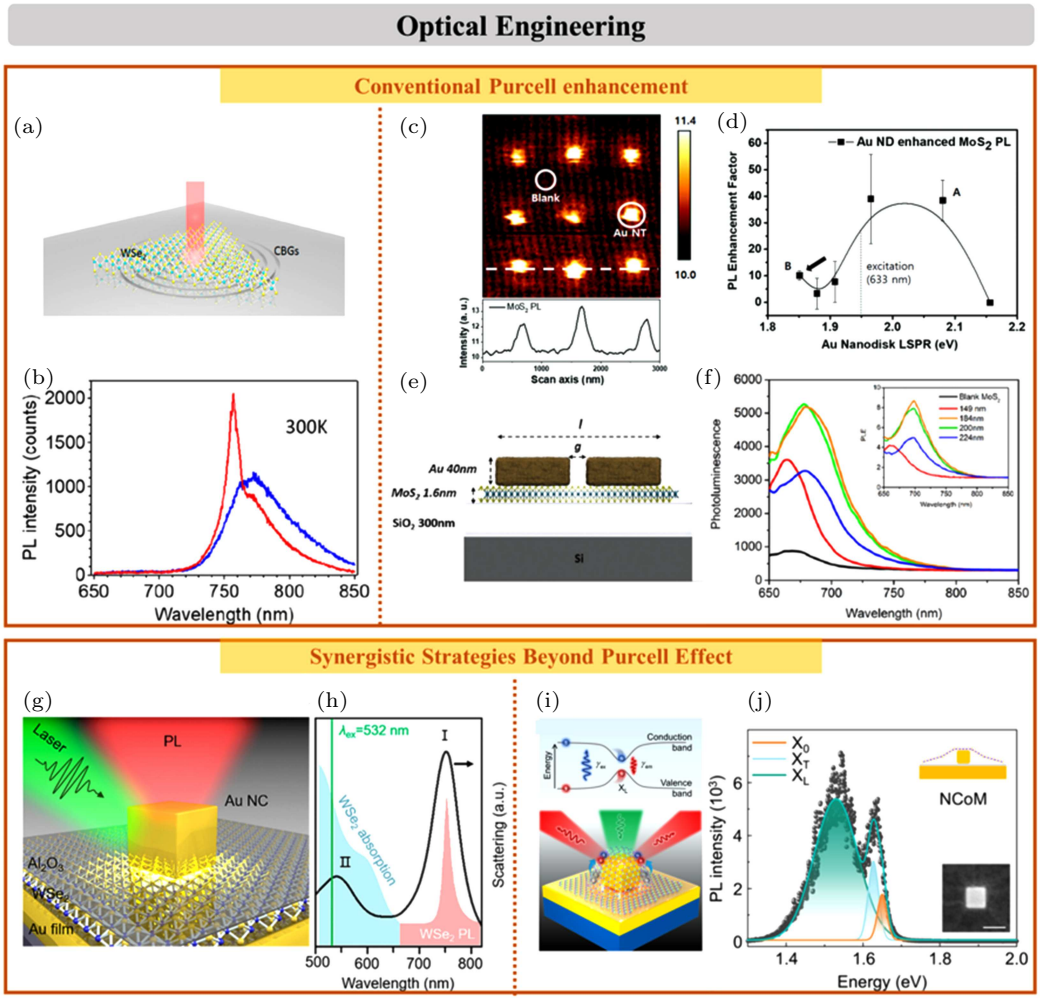


Fig. 6. (a) Schematic illustration and scanning electron microscopy image of the circular Bragg grating structure. (b) Comparison of room-temperature photoluminescence spectra of monolayer WSe_2 on and off the grating.[105] (c) Stage raster scanned PL image of a MoS_2 layer on an Au NT array (top), cross-section profile of PL intensity (bottom) was obtained along the line (white dash). (d) LSPR mode dependent PL enhancement factors modified by nanostructure area factor correction.[106] (e) Scanning electron microscopy image of dipole Au nanoantennas. (f) Photoluminescence enhancement spectra of monolayer MoS_2 under different dipole antenna configurations.[107] (g) Schematic of the double-resonant Au nanocube-on-mirror nanocavity for WSe_2. (h) Absorption, PL, and scattering spectra showing spectral overlap.[108] (i) Schematic of strain-induced localized exciton generation in a WSe_2-capped nanocavity. The energy diagram illustrates exciton localization within a potential well induced by local strain from the nanocube. (j) PL spectrum of WSe_2 monolayer showing neutral exciton, trion, and localized exciton peaks.[109] Reproduced with permission from Refs. [105–109].

On the other hand, the aforementioned metallic nanostructure modifications typically involve plasmonic arrays, which host complex interactions, including near-field coupling, far-field radiative coupling, and surface plasmon polaritons (SPPs), making it difficult to quantify the Purcell effect precisely. To address this, Palacios *et al*. employed single Au nanoantennas to study the enhancement effect of the near-field Purcell effect within the antenna gap on monolayer MoS_2 PL (Figs. 6(e) and 6(f)).[107] The research identified the antenna gap distance as the most critical parameter for modulating the Purcell effect. As the gap decreases, the local field intensifies sharply, and the corresponding Purcell factor increases accordingly. Ultimately, the experiment measured a peak PL enhancement of 8-fold using bow-tie antennas.

3.5.2. Synergistic strategies beyond Purcell effect

Relying solely on the Purcell effect usually yields only a few-fold to tens-fold PL enhancement. In recent years, researchers have introduced additional physical mechanisms into plasmonic nanocavities, achieving enhancement factors far beyond the sole Purcell effect. Xiao *et al*. reported three types of metal nanostructure-on-mirror nanocavities. The first, based on an Au nanosphere-on-mirror nanocavity, achieved 1265-fold and 680-fold enhancements for neutral exciton and trion emission in monolayer WS_2, respectively.[110] The second, based on an Ag nanowire-on-mirror nanocavity, achieved 1840-fold PL enhancement in monolayer $MoSe_2$.[111] The third, based on an Au nanocube-on-mirror nanocavity, achieved 18000-fold PL enhancement in monolayer WSe_2 (as shown in Figs. 6(g) and 6(h)). The above three works involve synergistic enhancement from multiple physical mechanisms, mainly including: using plasmonic hotspots and double-resonance design to increase α, utilizing the Purcell effect combined with Fano resonance or plasmon–exciton intermediate coupling to enhance γ_r, and employing an Al_2O_3 spacer to suppress metal-induced γ_{nr}. Furthermore, Xiao *et al*. introduced strain engineering through the sharp corners of Au nanocube-on-mirror nanocavity, using exciton localization to suppress γ_{nr}, achieving a significant PL intensity increase (Figs. 6(i) and 6(j)).[109] In addition to the above physical mechanisms, some new phenomena, such as multiphoton-excitation resonance energy transfer between quantum dots and two-dimensional materials, are in principle beneficial for increasing α and thus hold promise for application in PL QY modulation.[112]

4. Strategies for suppressing EEA under high generation rates

As the optical excitation power increases, the exciton generation rate rises, and the factors affecting the PL QY will also change accordingly. Under high generation rates, excessive exciton density enhances exciton–exciton interactions, thereby triggering EEA. EEA is a four-body interaction in which one exciton is annihilated, transferring its energy to another exciton, thereby reducing the PL QY. In 2014, Sun *et al*. observed efficient EEA in monolayer MoS_2 through ultrafast transient absorption measurements.[53] Additionally, numerous studies have also reported the occurrence of EEA.[51,52,113–115] The EEA effect significantly reduces the QY under high carrier injection conditions. Therefore, suppressing EEA is crucial for the development of high-brightness and high-efficiency TMDC-based light-emitting devices.

Researchers have proposed various strategies to suppress the EEA effect.[114] In 2017, Hoshi *et al*. discovered that simple hBN encapsulation could reduce the EEA rate constant by two orders of magnitude in WS_2, leading to a remarkable enhancement of PL intensity under high excitation power densities,[116] as shown in Figs. 7(a)–7(c). Compared to unencapsulated WS_2 on SiO_2, hBN encapsulation reduced the surface roughness of SiO_2 and the potential fluctuations induced by ionized impurities in WS_2. This facilitated the delocalization of excitons, which suppressed exciton–exciton interactions and lowered the probability of EEA.

In 2021, Lee *et al*. designed a structure with proximal metallic screening effects, as shown in Fig. 7(d), using an ultra-flat gold (Au) thin film substrate and isolating the Au film from WS_2 with multilayer hBN.[51] The formation of image dipoles in the Au film transformed the original dipolar exciton–exciton interaction into a quadrupole–quadrupole interaction, effectively screening the exciton–exciton interaction and suppressing EEA (Fig. 7(e)), leading to increased PL intensity. Figure 7(f) compares the absolute QY of monolayer WS_2 on a 7 nm hBN/Au substrate versus a SiO_2 substrate. The results indicate that, for both substrates, PL intensity decreases with increasing exciton generation rate; however, at high excitation levels, the hBN/Au substrate exhibits a less pronounced decline compared to the SiO_2 substrate. Specifically, at generation rates of approximately 6.8×10^{16} $cm^{-2}\cdot s^{-1}$ and 7.5×10^{20} $cm^{-2}\cdot s^{-1}$, the absolute PL intensity on the hBN/Au substrate is enhanced by factors of 3 and 18, respectively, relative to the SiO_2 substrate.

In 2022, Uddin *et al*. explored the use of strain engineering and found that applying a small tensile strain to WSe_2 could significantly enhance the PL QY while suppressing the reduction of PL QY at high excitation powers (Figs. 8(a)–8(c)).[117] Figure 8(b) shows the effect of different strain levels on PL intensity. Uddin *et al*. suggested that the strain could alter the band structure and inhibit van Hove singularity resonance at twice the exciton transition energy (EX) in the joint density of states, thus suppressing EEA. As the strain in WSe_2 increased, the PL QY improved significantly. At a strain level of 1.0% in WSe_2, a gate voltage of -20 V enabled the achievement of nearly unity PL QY, with the PL QY exhibiting a roll-off-free characteristic across all generation rates (Fig. 6(c)).

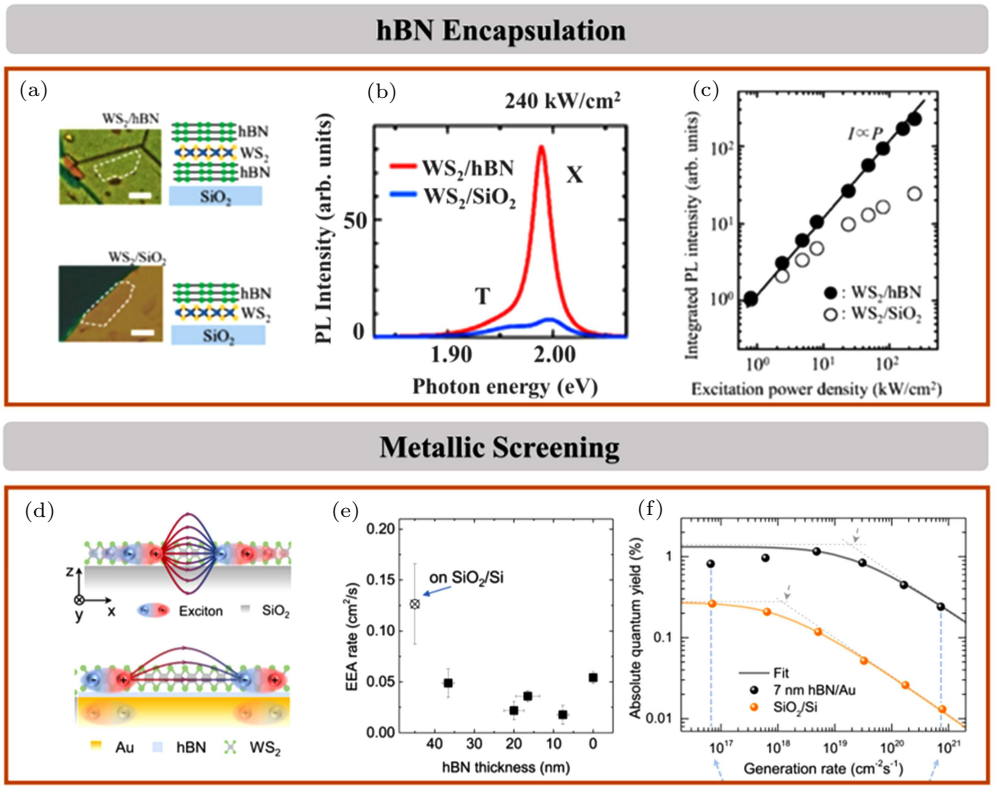


Fig. 7. (a) Schematic diagram of the structures of WS_2/hBN and WS_2/SiO_2 samples. (b) Steady-state PL spectra of WS_2/hBN (red) and WS_2/SiO_2 (blue). (c) PL intensity as a function of excitation power density for WS_2/hBN (solid circles) and WS_2/SiO_2 (open circles). (d) Schematic illustration of the suppression of exciton–exciton interactions by the hBN/Au substrate. Shaded arrows represent exciton–exciton interactions. Sparse field lines schematically indicate the weakening of exciton–exciton interactions due to the mirror dipole effect. (e) Relationship between the EEA rate and hBN thickness for monolayer WS_2 on hBN/Au (black squares) and SiO_2/Si (crossed circles) substrates. (f) Absolute PL QY as a function of generation rate for 1L-WS_2 on a 7 nm hBN/Au substrate (black dots) and a SiO_2/Si substrate (orange dots). Reproduced with permission from Refs. [51,116].

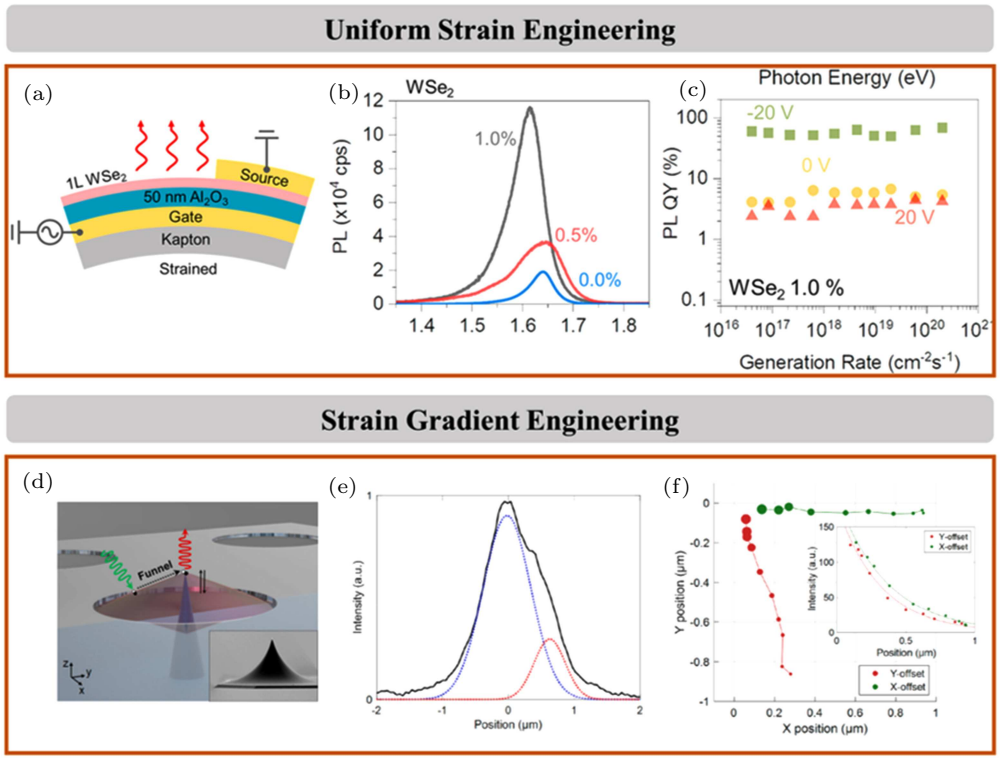


Fig. 8. (a) Schematic of the device used to explore PL. (b) PL spectra of monolayer WSe_2 under different uniaxial strain levels ($\varepsilon = 0\%$, 0.5%, and 1.0%) at a high generation rate of 2.2×10^{20} $cm^{-2}\cdot s^{-1}$ and a gate voltage of -20 V. The top-left inset shows a schematic of the strained device, while the top-right inset illustrates the EEA process. (c) PL QY of monolayer WSe_2 at different generation rates and gate voltages for a strain of $\varepsilon = 1.0\%$. (d) A schematic shows dynamic exciton flux control in a suspended two-dimensional semiconductor. (e) Wide-field PL images without (top) and with (middle) indentation, and their difference (bottom). (f) Funneled exciton position following excitation spot movement. Reproduced with permission from Refs. [117,119].

In addition to the global uniform strain induced by substrate deformation mentioned above, when a localized strain field is introduced into TMDCs through atomic force microscopy (AFM) tip indentation or nanopillar arrays, the band structure within the strained region is locally modulated, forming an energy potential well.[118] During diffusion, excitons migrate toward lower-energy regions and are captured and localized by the strain-induced potential well — this phenomenon is known as the "exciton funneling" effect. Moon *et al.*[119] realized dynamic exciton funneling in suspended monolayer WSe_2 using an AFM tip. By precisely controlling the strain gradient through tip displacement, they guided excitons to drift directionally over distances of several hundred nanometers. The strain-gradient-induced redistribution of excitons reduces the local exciton density near the excitation spot, thereby effectively suppressing EEA and enhancing the PL intensity (Figs. 8(d)–8(f)).

5. Conclusions and outlook

As atomically thin direct-bandgap semiconductors, TMDCs exhibit tremendous potential in the field of light-emitting materials. However, due to multiple limiting factors, even mechanically exfoliated TMDCs typically possess intrinsically low PL QY (< 10%), which is insufficient for practical applications. Over the past decade, significant progress has been made in understanding the photophysical mechanisms, influencing factors, and regulation strategies of PL in TMDCs. Centered on exciton formation probability, nonradiative recombination rates, and radiative recombination rates, numerous technical approaches have been proposed to enhance the PL QY of TMDCs under low excitation density conditions, including chemical doping, electrostatic doping, defect engineering, interface engineering, and optical engineering. Figure 9 summarizes the development of modulation techniques for PL intensity in TMDCs.

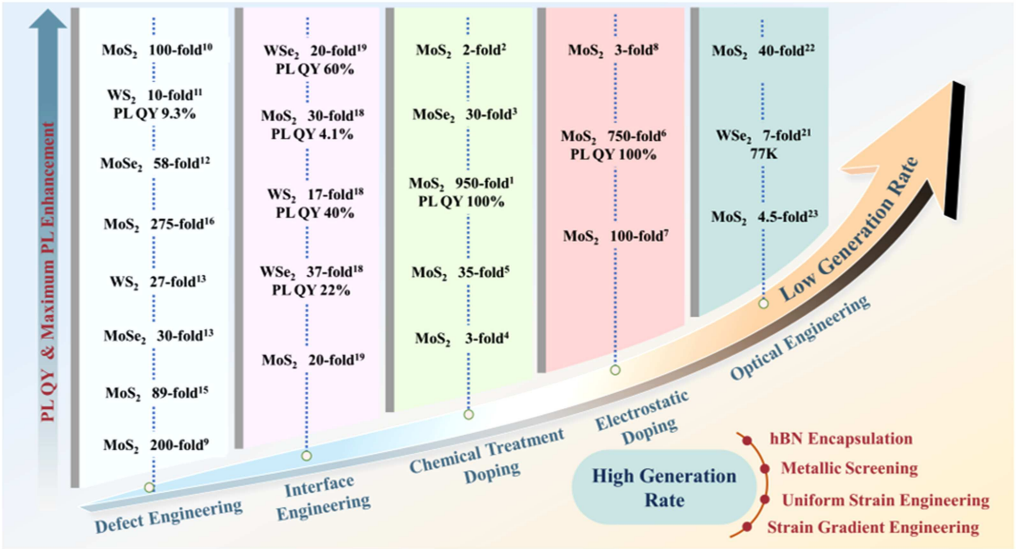


Fig. 9. Development of modulation techniques for PL intensity in TMDCs.[11,51,56–58,64–67,72,83,85,88–91,93,94,98,102,105–107,116–119]

Among these, studies on chemical and electrostatic doping have shown that even in the presence of defects, a simple doping-induced conversion of exciton species from charged excitons (trions) to neutral excitons is sufficient to increase the PL QY of MoS_2 and WS_2 to nearly 100%.[11,56] This finding opens promising prospects for the application of TMDCs in high-efficiency light-emitting devices. On the other hand, the atomic thickness and weak dielectric screening of TMDCs not only limit exciton diffusion lengths but also enhance Coulomb interactions between excitons, making EEA the primary factor restricting their application in high-brightness light emission. Encouragingly, various techniques have been developed to suppress EEA, such as hBN encapsulation, metallic image-dipole screening, and strain engineering, which mitigate the reduction of PL QY under high generation rates. In particular, strain engineering based on flexible substrates has even demonstrated a roll-off-free characteristic within the experimental range,[117] further consolidating the foundation for the engineering application of TMDC materials.

Despite substantial progress, several challenges remain before TMDCs can be practically implemented in light-emitting applications. First, although nearly 100% PL QY has been achieved in sulfur-based TMDCs, the chemical or electrostatic doping methods employed often possess specific constraints, which may greatly limit their practical applicability. Second, the understanding of the underlying physical mechanisms still requires further improvement. For instance, studies have shown that doping strategies are far less effective in enhancing the PL QY of selenide-based TMDCs, indicating that neutral excitons in TMDCs are not universally immune

to all types of defects. Third, most reports of high PL QY are based on mechanically exfoliated TMDCs. For scalable applications, CVD-grown TMDCs are clearly preferred; however, compared with high-quality exfoliated samples, CVD-grown TMDCs typically contain a higher density and diversity of defects,[87] further increasing the difficulty of PL QY regulation. Finally, practical applications require not only a high PL QY but also minimal efficiency roll-off with increasing generation rates. At present, however, research on enhancing PL intensity and suppressing EEA remains insufficiently integrated.

It is evident that relying on a single technical approach to simultaneously address these challenges is unrealistic. Therefore, future development in TMDC PL research should focus on synergistic multi-strategy approaches. Taking CVD-grown monolayer TMDCs as an example, suppressing non-radiative channels and enhancing radiative recombination require simultaneous consideration of defect passivation, strain release, doping modulation, etc., which inevitably involves multiple strategies, such as defect engineering, interface engineering, chemical treatment, and optical structure design. Several such collaborative strategies have already been reported. For example, Bretscher *et al.*[93] proposed combining defect passivation with doping during chemical treatment; Abramov *et al.*[120] introduced a PL regulation strategy based on the synergistic effects of localized strain and defects; and Koo *et al.*[121] developed a tip-enhanced PL technique, in which an Au tip serves simultaneously as a plasmonic resonant cavity and a strain-inducing tool. We believe that the continued development of such synergistic multi-technology strategies will not only accelerate the maturation and practical implementation of PL regulation techniques but also greatly facilitate a deeper understanding of the underlying physical mechanisms.

Acknowledgements

This work was supported by the National Key &D Program of China (Grant No. 2021YFC2202500) and the Interdisciplinary Research Program of HUST (Grant No. 2024JCYJ063).

References

[1] Zhou S, Ye Y, Ding K, Jiang D, Dou X and Sun B 2018 *Chin. Phys. Lett.* **35** 066201
[2] Voshell A, Terrones M and Rana M 2018 *Proc. of SPIE* **10754** 107540L
[3] Komsa H P and Krasheninnikov A V 2012 *J. Phys. Chem. Lett.* **3** 3652
[4] Bernardi M, Palummo M and Grossman J C 2013 *Nano Lett.* **13** 3664
[5] Queisser H J and Haller E E 1998 *Science* **281** 945
[6] Scholes G D and Rumbles G 2006 *Nat. Mater.* **5** 683
[7] Deilmann T and Thygesen K S 2017 *Phys. Rev. B* **96** 201113
[8] Gusakova J, Wang X, Shiau L, Krivosheeva A, Shaposhnikov V, Borisenko V, Gusakov V and Tay B K 2017 *Physica Status Solidi (a)* **214** 1700218
[9] Ridolfi E, Lewenkopf C H and Pereira V M 2018 *Phys. Rev. B* **97** 205409
[10] Li J, Yang R, Li R and Grigoropoulos C P 2025 *Adv. Opt. Mater.* **13** 2403137
[11] Lien D H, Uddin S Z, Yeh M, Amani M, Kim H, Ager J W, Yablonovitch E and Javey A 2019 *Science* **364** 468
[12] You Y, Zhang X X, Berkelbach T C, Hybertsen M S, Reichman D R and Heinz T F 2015 *Nat. Phys.* **11** 477
[13] Steinhoff A, Florian M, Singh A, Tran K, Kolarczik M, Helmrich S, Achtstein A W, Woggon U, Owschimikow N, Jahnke F and Li X 2018 *Nat. Phys.* **14** 1199
[14] Rivera P, Schaibley J R, Jones A M, Ross J S, Wu S, Aivazian G, Klement P, Seyler K, Clark G, Ghimire N J, Yan J, Mandrus D G, Yao W and Xu X 2015 *Nat. Commun.* **6** 6242
[15] Yu H, Liu G B, Tang J, Xu X and Yao W 2017 *Sci. Adv.* **3** e1701696
[16] Ross J S, Wu S, Yu H, Ghimire N J, Jones A M, Aivazian G, Yan J, Mandrus D G, Xiao D, Yao W and Xu X 2013 *Nat. Commun.* **4** 1474
[17] Plechinger G, Nagler P, Kraus J, Paradiso N, Strunk C, Schüller C and Korn T 2015 **9** 457
[18] Berkelbach T, Hybertsen M and Reichman D 2013 *Phys. Rev. B* **88** 045318
[19] Chen X, Lian Z, Meng Y, Ma L and Shi S F 2023 *Nat. Commun.* **14** 8233
[20] Echeverry J P, Urbaszek B, Amand T, Marie X and Gerber I C 2016 *Phys. Rev. B* **93** 121107
[21] Lo T W, Zhang Q, Qiu M, Guo X, Meng Y, Zhu Y, Xiao J J, Jin W, Leung C W and Lei D 2019 *ACS Photon.* **6** 411
[22] Lo T W, Chen X, Zhang Z, Zhang Q, Leung C W, Zayats A V and Lei D 2022 *Nano Lett.* **22** 191
[23] Hu Z, Wu Z, Han C, He J, Ni Z and Chen W 2018 *Chem. Soc. Rev.* **47** 3100
[24] Zhang Y, Li H, Wang H, Liu R, Zhang S L and Qiu Z J 2015 *ACS Nano* **9** 8514
[25] Christopher J W, Goldberg B B and Swan A K 2017 *Sci. Rep.* **7** 14062
[26] Cheng Y, Wang J Z, Wei X X, Guo D, Wu B, Yu L W, Wang X R and Shi Y 2015 *Chin. Phys. Lett.* **32** 117801
[27] Yu Y, Hu S, Su L, Huang L, Liu Y, Jin Z, Purezky A A, Geohegan D B, Kim K W, Zhang Y and Cao L 2015 *Nano Lett.* **15** 486
[28] Fogler M M, Butov L V and Novoselov K S 2014 *Nat. Commun.* **5** 4555
[29] Gao S, Yang L and Spataru C D 2017 *Nano Lett.* **17** 7809
[30] Nagler P, Plechinger G, Ballottin M V, Mitioglu A, Meier S, Paradiso N, Strunk C, Chernikov A, Christianen P C M, Schüller C and Korn T 2017 *2D Mater.* **4** 025112
[31] Baranowski M, Surrente A, Klopotowski L, Urban J M, Zhang N, Maude D K, Wiwatowski K, Mackowski S, Kung Y C, Dumcenco D, Kis A and Plochocka P 2017 *Nano Lett.* **17** 6360
[32] Fang H, Battaglia C, Carraro C, Nemsak S, Ozdol B, Kang J S, Bechtel H A, Desai S B, Kronast F, Unal A A, Conti G, Conlon C, Palsson G K, Martin M C, Minor A M, Fadley C S, Yablonovitch E, Maboudian R and Javey A 2014 *Proc. Natl. Acad. Sci. USA* **111** 6198
[33] Ovesen S, Brem S, Linderälv C, Kuisma M, Korn T, Erhart P, Selig M and Malic E 2019 *Commun. Phys.* **2** 23
[34] Mouri S, Zhang W, Kozawa D, Miyauchi Y, Eda G and Matsuda K 2017 *Nanoscale* **9** 6674
[35] Miller B, Steinhoff A, Pano B, Klein J, Jahnke F, Holleitner A and Wurstbauer U 2017 *Nano Lett.* **17** 5229
[36] Jiang Y, Chen S, Zheng W, Zheng B and Pan A 2021 *Light Sci. Appl.* **10** 72
[37] Hong X, Kim J, Shi S F, Zhang Y, Jin C, Sun Y, Tongay S, Wu J, Zhang Y and Wang F 2014 *Nat. Nanotech.* **9** 68
[38] Peimyoo N, Yang W, Shang J, Shen X, Wang Y and Yu T 2014 *ACS Nano* **8** 11320
[39] Chow P K, Jacobs-Gedrim R B, Gao J, Lu T M, Yu B, Terrones H and Koratkar N 2015 *ACS Nano* **9** 1520
[40] Tongay S, Suh J, Ataca C, Fan W, Luce A, Kang J S, Liu J, Ko C, Raghunathanan R, Zhou J, Ogletree F, Li J, Grossman J C and Wu J 2013 *Sci. Rep.* **3** 2657
[41] Yuan S, Roldán R, Katsnelson M I and Guinea F 2014 *Phys. Rev. B* **90** 041402
[42] Zhang S, Wang C G, Li M Y, Huang D, Li L J, Ji W and Wu S 2017 *Phys. Rev. Lett.* **119** 046101
[43] Kumar R, Verzhbitskiy I and Eda G 2015 *Strong IEEE Journal of Quantum Electronics* **51** 0600206
[44] Yu Y, Dang J, Qian C, Sun S, Peng K, Xie X, Wu S, Song F, Yang J, Xiao S, Yang L, Wang Y, Shan X, Rafiq M A, Li B B and Xu X 2019 *Phys. Rev. Mater.* **3** 051001

[45] Lee Y, Yun S J, Kim Y, Kim M S, Han G H, Sood A K and Kim J 2017 *Nanoscale* **9** 2272

[46] Venanzi T, Arora H, Erbe A, Pashkin A, Winnerl S, Helm M and Schneider H 2019 *Appl. Phys. Lett.* **114** 172106

[47] Komsa H P, Kotakoski J, Kurasch S, Lehtinen O, Kaiser U and Krasheninnikov A V 2012 *Phys. Rev. Lett.* **109** 035503

[48] Zhang Y, Ma K, Zhao C, Hong W, Nie C, Qiu Z J and Wang S 2021 *ACS Nano* **15** 4405

[49] Chee S S, Lee W J, Jo Y R, Cho M K, Chun D W, Baik H, Kim B J, Yoon M H, Lee K and Ham M H 2020 *Adv. Funct. Mater.* **30** 1908147

[50] McMahon J M, Kioupakis E and Schulz S 2023 *J. Phys. D: Appl. Phys.* **57** 125102

[51] Lee Y, Forte J D S, Chaves A, Kumar A, Tran T T, Kim Y, Roy S, Taniguchi T, Watanabe K, Chernikov A, Jang J I, Low T and Kim J 2021 *Nat. Commun.* **12** 7095

[52] Wang G, Marie X, Bouet L, Vidal M, Balocchi A, Amand T, Lagarde D and Urbaszek B 2014 *Appl. Phys. Lett.* **105** 182105

[53] Sun D, Rao Y, Reider G A, Chen G, You Y, Brézin L, Harutyunyan A R and Heinz T F 2014 *Nano Lett.* **14** 5625

[54] Amani M, Taheri P, Addou R, Ahn G H, Kiriya D, Lien D H, Ager J W, Wallace R M and Javey A 2016 *Nano Lett.* **16** 2786

[55] Lin Y C, Björkman T, Komsa H P, Teng P Y, Yeh C H, Huang F S, Lin K H, Jadczak J, Huang Y S, Chiu P W, Krasheninnikov A V and Suenaga K 2015 *Nat. Commun.* **6** 6736

[56] Amani M, Lien D H, Kiriya D, Xiao J, Azcatl A, Noh J, Madhvapathy S R, Addou R, Kc S, Dubey M, Cho K, Wallace R M, Lee S C, He J H, Ager J W, Zhang X, Yablonovitch E and Javey A 2015 *Science* **350** 1065

[57] Kim H, Ahn G, Cho J, Amani M, Mastandrea J, Groschner C, Lien D H, Zhao Y, Ager J, Scott M, Chrzan D and Javey A 2019 *Sci. Adv.* **5** eaau4728

[58] Tanoh A O A, Alexander-Webber J, Fan Y, Gauriot N, Xiao J, Pandya R, Li Z, Hofmann S and Rao A 2021 *Nanoscale Adv.* **3** 4216

[59] Wang Y, Zheng Y, Han C and Chen W 2021 *Nano Research* **14** 1682

[60] Yan-Tao S, You-Wei Z and Shun W 2021 *Acta Phys. Sin.* **70** 177301 (in Chinese)

[61] Li Z, Bretscher H, Zhang Y, Delport G, Xiao J, Lee A, Stranks S D and Rao A 2021 *Nat. Commun.* **12** 6044

[62] Kiriya D and Lien D H 2022 *Nano Ex.* **3** 034002

[63] Su W, Dou H, Li J, Huo D, Dai N and Yang L 2015 *RSC Adv.* **5** 8292

[64] Zhang S, Hill H M, Moudgil K, Richter C A, Hight Walker A R, Barlow S, Marder S R, Hacker C A and Pookpanratana S J 2018 *Adv. Mater.* e1802991

[65] Han H V, Lu A Y, Lu L S, Huang J K, Li H, Hsu C L, Lin Y C, Chiu M H, Suenaga K, Chu C W, Kuo H C, Chang W H, Li L J and Shi Y 2016 *ACS Nano* **10** 1454

[66] Mouri S, Miyauchi Y and Matsuda K 2013 *Nano Lett.* **13** 5944

[67] Tongay S, Zhou J, Ataca C, Liu J, Kang J S, Matthews T S, You L, Li J, Grossman J C and Wu J 2013 *Nano Lett.* **13** 2831

[68] Durán Retamal J R, Periyanagounder D, Ke J J, Tsai M L and He J H 2018 *Chem. Sci.* **9** 7727

[69] Zhang Y, Shen W, Wu S, Tang W, Shu Y, Ma K, Zhang B, Zhou P and Wang S 2022 *ACS Nano* **16** 19187

[70] Ruiheng C, Chen Q, Shen W, Zhang Y, Zhang B and Wang S 2023 *Adv. Funct. Mater.* **33** 2301010

[71] Li Z, Chang S W, Chen C C and Cronin S B 2014 *Nano Res.* **7** 97

[72] Newaz A K M, Prasai D, Ziegler J I, Caudel D, Robinson S, Haglund Jr. R F and Bolotin K I 2013 *Solid State Commun.* **155** 49

[73] Wu S, Ross J S, Liu G B, Aivazian G, Jones A, Fei Z, Zhu W, Xiao D, Yao W, Cobden D and Xu X 2013 *Nat. Phys.* **9** 149

[74] Yang J, Lü T, Myint Y W, Pei J, Macdonald D, Zheng J C and Lu Y 2015 *ACS Nano* **9** 6603

[75] Jones A M, Yu H, Ghimire N J, Wu S, Aivazian G, Ross J S, Zhao B, Yan J, Mandrus D G, Xiao D, Yao W and Xu X 2013 *Nat. Nanotech.* **8** 634

[76] Shang J, Shen X, Cong C, Peimyoo N, Cao B, Eginligil M and Yu T 2015 *ACS Nano* **9** 647

[77] Addou R, Colombo L and Wallace R M 2015 *ACS Appl. Mater. Interfaces* **7** 11921

[78] Herzog A H, Keune D L and Craford M G 1972 *J. Appl. Phys.* **43** 600

[79] Schilling M, Hartmann C, Guttmann M, Juda U, Muhin A, Hpfner J, Wernicke T, Straubinger T and Kneissl M 2025 *Phys. Status Solidi A-Appl. Mat.* **222** 2400812

[80] Quevedo A, Wu F, Tsai T Y, Ewing J J, Tak T, Gandrothula S, Gee S, Li X, Nakamura S, DenBaars S P and Speck J S 2024 *Appl. Phys. Lett.* **125** 042104

[81] Le L C, Zhao D G, Jiang D S, Li L, Wu L L, Chen P, Liu Z S, Li Z C, Fan Y M, Zhu J J, Wang H, Zhang S M and Yang H 2012 *Appl. Phys. Lett.* **101** 252110

[82] Zhang Y, Wang J, Nong H, He L, Li S, Wei Q, Wu Q and Liu B 2024 *Adv. Funct. Mater.* **34** 2410402

[83] Tanoh A O A, Alexander-Webber J, Xiao J, Delport G, Williams C A, Bretscher H, Gauriot N, Allardice J, Pandya R, Fan Y, Li Z, Vignolini S, Stranks S D, Hofmann S and Rao A 2019 *Nano Lett.* **19** 6299

[84] Cheng J, Yuan J H, Li P Y, Wang J, Wang Y, Zhang Y W, Zheng Y and Zhang P 2024 *ACS Appl. Mater. Interfaces* **16** 24987

[85] Pucher T, Puebla S, Zamora V, Sánchez Viso E, Rouco V, Leon C, Garcia-Hernandez M, Santamaria J, Munuera C and Castellanos-Gomez A 2024 *Adv. Funct. Mater.* **34** 2409447

[86] Vancsó P, Magda G Z, Pető J, Noh J Y, Kim Y S, Hwang C, Biró L P and Tapasztó L 2016 *Sci. Rep.* **6** 29726

[87] Hong J, Hu Z, Probert M, Li K, Lv D, Yang X, Gu L, Mao N, Feng Q, Xie L, Zhang J, Wu D, Zhang Z, Jin C, Ji W, Zhang X, Yuan J and Zhang Z 2015 *Nat. Commun.* **6** 6293

[88] Wei X, Yu Z, Hu F, Cheng Y, Yu L, Wang X, Xiao M, Wang J, Wang X and Shi Y 2014 *AIP Adv.* **4** 123004

[89] Chen Y, Huang Z, Liu H, Yu G, Zhang J, Xu Z, Chen M, Li D, Ma C, Huang M, Zhu X, Chen S, Jiang Y and Pan A 2024 *Sci. China Mater.* **67** 2232

[90] Cui Q, Luo Z, Cui Q, Zhu W, Shou H, Wu C, Liu Z, Lin Y, Zhang P, Wei S, Yang H, Chen S, Pan A and Song L 2021 *Adv. Funct. Mater.* **31** 2105339

[91] Nan H, Wang Z, Wang W, Liang Z, Lu Y, Chen Q, He D, Tan P, Miao F, Wang X, Wang J and Ni Z 2014 *ACS Nano* **8** 5738

[92] Zhang X, Liao Q, Liu S, Kang Z, Zhang Z, Du J, Li F, Zhang S, Xiao J, Liu B, Ou Y, Liu X, Gu L and Zhang Y 2017 *Nat. Commun.* **8** 15881

[93] Bretscher H, Li Z, Xiao J, Qiu D Y, Refaely-Abramson S, Alexander-Webber J A, Tanoh A, Fan Y, Delport G, Williams C A, Stranks S D, Hofmann S, Neaton J B, Louie S G and Rao A 2021 *ACS Nano* **15** 8780

[94] Xu W, Li S, Zhou S, Lee J K, Wang S, Sarwat S G, Wang X, Bhaskaran H, Pasta M and Warner J H 2018 *ACS Appl. Mater. Interfaces* **10** 4630

[95] Xu W, Kozawa D, Zhou Y, Wang Y, Sheng Y, Jiang T, Strano M S and Warner J H 2020 *Small* **16** 1905985

[96] Zheng B, Zheng W, Jiang Y, Chen S, Li D, Ma C, Wang X, Huang W, Zhang X, Liu H, Jiang F, Li L, Zhuang X, Wang X and Pan A 2019 *J. Am. Chem. Soc.* **141** 11754

[97] Yu Y, Li G, Huang L, Barrette A, Cai Y Q, Yu Y, Gundogdu K, Zhang Y W and Cao L 2017 *ACS Nano* **11** 9390

[98] Yu Y, Yu Y, Xu C, Cai Y, Su L, Zhang Y, Zhang Y W, Gundogdu K and Cao L 2016 *Adv. Funct. Mater.* **26** 4733

[99] Buscema M, Steele G A, van der Zant H S J and Castellanos-Gomez A 2014 *Nano Res.* **7** 561

[100] Golovynskyi S, Irfan I, Bosi M, Seravalli L, Datsenko O I, Golovynska I, Li B, Lin D and Qu J 2020 *Appl. Sur. Sci.* **515** 146033

[101] Sharma S, Bhagat S, Singh J, Ahmad M and Sharma S 2018 *J. Mater. Sci: Mater. Electron* **29** 20064

[102] Lin Y, Ling X, Yu L, Huang S, Hsu A L, Lee Y H, Kong J, Dresselhaus M S and Palacios T 2014 *Nano Lett.* **14** 5569

[103] Liu Z, Amani M, Najmaei S, Xu Q, Zou X, Zhou W, Yu T, Qiu C, Birdwell A G, Crowne F J, Vajtai R, Yakobson B I, Xia Z, Dubey M, Ajayan P M and Lou J 2014 *Nat. Commun.* **5** 5246

[104] Tran M D, Kim J H and Lee Y H 2016 *Current Applied Physics* **16** 1159

[105] Duong N M H, Xu Z Q, Kianinia M, Su R, Liu Z, Kim S, Bradac C, Tran T T, Wan Y, Li L J, Solntsev A, Liu J and Aharonovich I 2018 *ACS Photon.* **5** 3950

[106] Kim H, Moon S, Kim J, Nam S H, Kim D H, Lee J S, Kim K H, Kang E S H, Ahn K J, Kim T, Shin C and Suh Y D 2021 *Nanoscale* **13** 5316

[107] Palacios E, Park S, Butun S, Lauhon L and Aydin K 2017 *Appl. Phys. Lett.* **111** 031101

[108] Li C, Luo H, Hou L, Wang Q, Liu K, Gan X, Zhao J and Xiao F 2024 *Nano Lett.* **24** 5879

[109] Wang Q, Xue G, Ji C, Li Y, Li C, Hou L, Zheng X, Yu Q, Ma C, Gan X, Liu K, Zhao J and Xiao F 2026 *ACS Nano* **20** 6279
[110] Hou L, Wang Q, Zhang H, Wang P, Gan X, Xiao F and Zhao J 2022 *APL Photon.* **7** 026107
[111] Li C, Wang Q, Diao H, Hao Z, Yu W, Liu K, Gan X, Xiao F and Zhao J 2022 *Laser & Photonics Reviews* **16** 2100199
[112] Hong H, Wu C, Zhao Z, Zuo Y, Wang J, Liu C, Zhang J, Wang F, Feng J, Shen H, Yin J, Wu Y, Zhao Y, Liu K, Gao P, Meng S, Wu S, Sun Z, Liu K and Xiong J 2021 *Nat. Photon.* **15** 510
[113] Ye Y, Ye Z, Gharghi M, Zhu H, Zhao M, Wang Y, Yin X and Zhang X 2014 *Appl. Phys. Lett.* **104** 193508
[114] Lee Y and Kim J 2018 *ACS Photon.* **5** 4187
[115] Yuan L and Huang L 2015 *Nanoscale* **7** 7402
[116] Hoshi Y, Kuroda T, Okada M, Moriya R, Masubuchi S, Watanabe K, Taniguchi T, Kitaura R and Machida T 2017 *Phys. Rev. B* **95** 241403
[117] Uddin S Z, Higashitarumizu N, Kim H, Rahman I K M R and Javey A 2022 *Nano Lett.* **22** 5316
[118] Harats M G and Bolotin K I 2020 *2D Mater.* **8** 015010
[119] Moon H, Grosso G, Chakraborty C, Peng C, Taniguchi T, Watanabe K and Englund D 2020 *Nano Lett.* **20** 6791
[120] Abramov A N, Chestnov I Y, Alimova E S, Ivanova T, Mukhin I S, Krizhanovskii D N, Shelykh I A, Iorsh I V and Kravtsov V 2023 *Nat. Commun.* **14** 5737
[121] Koo Y, Kim Y, Choi S H, Lee H, Choi J, Lee D Y, Kang M, Lee H S, Kim K K, Lee G and Park K D 2021 *Adv. Mater.* **33** 2008234